Evidence for an equilibrium epitaxial complexion at the Au-MgAl2O4 interface

Tahereh Majdi, Guo-zhen Zhu, Jessica Carvalho, Victoria Jarvis, Kristoffer Meinander, James F. Britten, Gianluigi Botton, and John S. Preston

Citation: Applied Physics Letters **107**, 241601 (2015); doi: 10.1063/1.4937430
View online: http://dx.doi.org/10.1063/1.4937430
View Table of Contents: http://scitation.aip.org/content/aip/journal/apl/107/24?ver=pdfcov
Published by the AIP Publishing

Evidence for an equilibrium epitaxial complexion at the Au-$MgAl_2O_4$ interface

Tahereh Majdi,[1] Guo-zhen Zhu,[2,a)] Jessica Carvalho,[1] Victoria Jarvis,[3] Kristoffer Meinander,[1] James F. Britten,[3] Gianluigi Botton,[2] and John S. Preston[1,b)]
[1]*Department of Engineering Physics, McMaster University, Hamilton, Ontario L8S 4L7, Canada*
[2]*Canadian Center for Electron Microscopy and Department of Materials Science and Engineering, McMaster University, 1280 Main Street West, Hamilton, Ontario L8S 4M1, Canada*
[3]*McMaster Analytical X-ray Diffraction Facility, Department of Chemistry, McMaster University, 1280 Main Street West, Hamilton, Ontario L8S 4M1, Canada*

(Received 5 July 2015; accepted 24 November 2015; published online 14 December 2015)

Evidence for the existence of an equilibrium epitaxial complexion at the Au-$MgAl_2O_4$ interface has been observed. The growth of crystalline $MgAl_2O_4$ nanostructures, from a previously stable substrate in the presence of an Au overlayer and heat, is associated with this complexion. Prior to the nanostructures' self-assembly, Au nanoparticles crystalize, then reorient to align with the $MgAl_2O_4$ substrate. The presented results contradict earlier conclusions based solely on SEM studies of the final assembled nanostructures. Those results suggested that the $MgAl_2O_4$ grown pedestal and associated Au nanoparticle atop were both gold. © *2015 AIP Publishing LLC*.
[http://dx.doi.org/10.1063/1.4937430]

The size dependent electrochemistry, optical properties, and high chemical stability of gold nanoparticles have made them an ideal choice for investigating and demonstrating a wide range of phenomena,[1] including self-assembly,[2–4] biolabeling,[5] catalysis,[6] electron-transfer theories,[7] phase transfer,[8] DNA melting,[9] nanowire,[10] and crystal growth.[11] Gold nanoparticles can be fabricated as stand-alone structures or in combination with a support structure. Oxides have received particular attention due to their structural differences and chemical-physical characteristics such as optical transparency in the visible range, insulating nature, structural and thermal stabilities, and weak interaction with the host.[12] Within the oxide family, magnesium aluminate spinel, $MgAl_2O_4$, has gained increasing interest in the past few years, particularly for application in catalysis, as a host material in combination with metal nanoparticles,[13–19] especially gold.[17,18,20–22] The prominent catalytic activity of gold is limited to nanoparticles smaller than 10 nm and is highly dependent on the route of synthesis and deposition, which may be similar to those employed in this work,[23] but mainly rely on preparation of well-mixed precursors, deposition, or adsorption of Au compounds.[24]

Previously, our group had studied the dewetting of Au films on $MgAl_2O_4$ substrates motivated by their near pseudo lattice match; spinel's lattice constant, 8.083 Å, is almost twice that of gold, 4.078 Å.[25] In 2009, Devenyi *et al.* reported on the unique, intricate self-assembly of gold nanostructures that are formed by dewetting gold films on magnesium aluminate substrates, using a two-step annealing profile involving temperatures near the melting point of gold. In that work, based on a scanning electron microscopy (SEM) study, it was assumed that the intricate structures were made entirely of gold;[25] thus, these structures remained an anomaly among reported dewetting and growth studies as their structures deviated vastly from the expected Wulff-like structures.

An extensive study on the Au/$MgAl_2O_4$ system and the findings that have followed are reported in this letter. In part, these findings come from mapping the structure type over a much broader range of annealing temperatures. More importantly, the structures are studied using high resolution scanning transmission electron microscopy (STEM) and three dimensional X-ray diffraction texture analysis (XRD3), in addition to SEM and atomic force microscopy (AFM). This added compositional and structural information makes it clear that the dewetted gold nanoparticles act as a seed causing crystalline $MgAl_2O_4$ structures to spontaneously grow underneath the gold nanoparticles, lifting them above the initial substrate surface. Associated with this self-assembly, an epitaxial bilayer is observed between the gold and the spinel. Finally, the formation of the bilayer and resulting spinel growth coincides with a strong epitaxial alignment of the three regions especially near the interface. Perhaps the most intriguing interpretation of these results is that the bilayer is a complexion formed to minimize the free energy cost of the transition from the spinel to gold structures. This interpretation, which represents an epitaxial complexion i.e., a complexion that is lattice matched to both adjacent phases, creates opportunities in the design of epitaxial heterostructures that are thermodynamically stable.

The specimens were prepared by sputtering a thin film of Au with a thickness between 5 Å–500 Å on a (111) $MgAl_2O_4$ substrate (MTI Corporation) and annealing them in a quartz tube furnace. Annealing was carried out in an argon atmosphere (99.9995% purity) with a flow of 100 ccm. The furnace readings were referenced to a bath of ice-water using a reference junction thermocouple. Au deposition was performed using a GATAN PECS Model 682 ion beam coating/etching system at room temperature. Following a typical annealing profile which led to the self-assembly of Au-$MgAl_2O_4$ nanostructures, the samples were heated to

[a)]Present address: School of Materials Science and Engineering, Shanghai Jiao Tong University, 800 Dongchuan Road, Shanghai 200030, People's Republic of China.
[b)]Author to whom correspondence should be addressed. Electronic mail: prestonj@mcmaster.ca

1110 °C in 1.5 h, soaked at this temperature for 1.5 h, then cooled to 965 °C in 0.5 h, and soaked here for 2 h. They were then left to cool to 30 °C over 14 h. The maximum temperature was varied between 640 °C to 1110 °C, and the initial and final soak durations were varied between 0 to 1.5 h and 0 to 2 h, respectively, in order to investigate the effect of temperature variations on the self-assembly of Au-$MgAl_2O_4$ nanostructures.

The evolution of the nanoparticle morphology was followed as a function of temperature and initial film thickness using a JEOL JSM-7000 F SEM in secondary electron mode, with the specimens tilted to 70°. Samples prepared with the same thickness of gold, but increasing annealing temperature and duration show progressive stages of dewetting, Ostwald-like ripening, and ultimately the formation of intricately shaped nanoparticles (Figures 1(a)–1(c)). Figure 1 also illustrates three dimensional texture data through stereographic projections of the {111} X-ray reflections from all orientations of the gold nanoparticles. The north of the pole figures represents the [1–21] direction of the substrate. Due to the epitaxial relationship between gold and $MgAl_2O_4$, all the pole figures include reflection contributions from the substrate. The pole figure on the top panel of Figure 1(a) shows the sharp peaks associated with the crystalline substrate while the contribution from the gold is a central peak and a diffuse ring. This is consistent with the gold being oriented with its [111] direction parallel to the [111] direction of the substrate but with random in-plane orientation. The higher heat treatment for the sample described by Figure 1(b) is responsible for radial sharpening of the diffuse ring as measured through XRD3, which indicates an enhanced alignment of the gold in the [111] direction. In contrast, for samples treated at 1110 °C, there is a clear qualitative change in both the shape of the nanostructures and crystallographic orientation. The pole figure indicates the presence of highly ordered gold nanoparticles with epitaxy dominating the preferential orientation of the gold nanoparticles such that $\{111\}_{Au}||\{111\}_{MgAl_2O_4}$ and $\langle 10\text{–}1\rangle_{Au}||\langle 10\text{–}1\rangle_{MgAl_2O_4}$. These orientations were confirmed by analyzing the {200} X-ray reflections of gold as well.

In order to probe the individual intricately shaped nanoparticles formed on the $MgAl_2O_4$ substrate, samples for cross-sectional microscopy were prepared by a Zeiss NVision 40 focused ion beam instrument/SEM. Using a spherical-aberration probe-corrected scanning transmission electron microscope (FEI Titan 80–300 HB) equipped with an electron energy loss spectrometer and annular bright-field and dark-field detectors, we investigate the chemical composition and atomic bonding configuration of the self-assembled nanoparticles based on the experimental conditions described in Ref. 26. The STEM-high-angle annular dark-field (HAADF) image in Figure 2 has distinct contrast within the composite nanostructure revealing that the structure is composed of three distinct regions: a faceted spherical structure, a necking region connecting it to the substrate, and a unique interfacial boundary layer. The necking structure formed below the gold nanoparticle has the same contrast as the $MgAl_2O_4$ substrate. In addition, this supporting structure extends the $MgAl_2O_4$ substrate lattice as shown in the high-resolution images. Energy dispersive X-ray spectroscopy measurements only detect the presence of magnesium, aluminum, and oxygen elements within the necking region and gold in the faceted spherical structure above it. The combined results suggest that the necking structure consists of purely magnesium aluminate, which epitaxially grows above the substrate surface, beneath a crystalline gold nanostructure, as a consequence of the annealing process. The distinct and unique interfacial boundary layer is crystalline, two monolayers thick, with only oxygen and gold identified as its constituent elements. We believe this bilayer is likely an

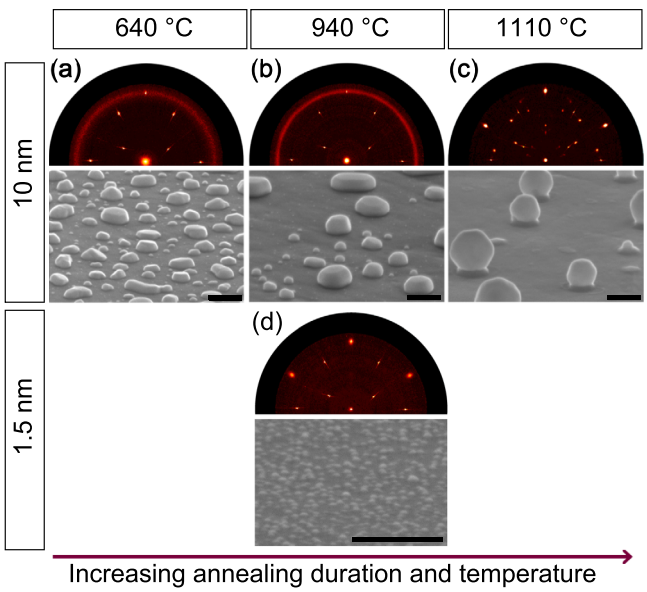

FIG. 1. The influence of annealing temperature and Au film thickness for films annealed on (111) $MgAl_2O_4$ substrates is shown through SEM micrographs and the corresponding (111) pole figures of the Au nanoparticles. Full pole figures were measured but are not presented due to their symmetry with the portion of the patterns shown. All SEM images were captured with specimens at a 70° tilt. The black scale bars are 200 nm.

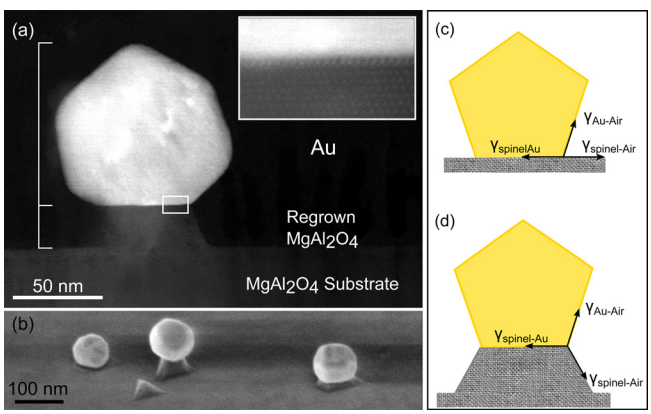

FIG. 2. (a) STEM High-angle annular dark field (HAADF) image of an Au-$MgAl_2O_4$ nanostructure self-assembled by annealing a gold film on a (111) $MgAl_2O_4$ substrate. The substrate is in a [1–10] projection. Inset: high resolution HAADF at the interface showing the complexion with Au atop and the epitaxially grown $MgAl_2O_4$ nanostructure beneath it. (b) SEM micrograph (Magellan 400) of the specimen at 50° tilt imaged prior to TEM measurements. (c) Schematic diagram showing negligible substrate mass transport when annealing at low temperatures for short durations. The vertical component of the Au-air interfacial tension, $\gamma_{Au\text{-}air}$, is balanced by inducing elastic stress in the substrate. (d) Annealing at sufficiently high temperatures for long enough durations facilitates substrate surface reconfiguration in favor of reducing stress.

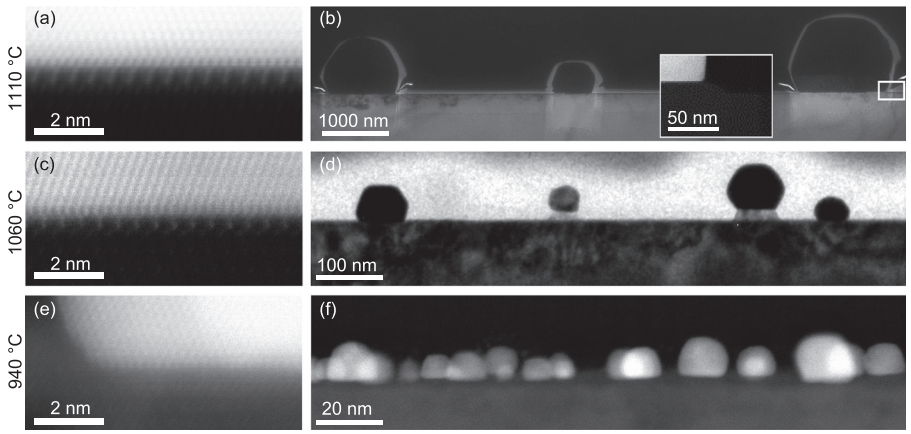

FIG. 3. STEM HAADF image of Au-$MgAl_2O_4$ interface for (a) 50 nm Au, annealed at 1110 °C for 1.5 h, and at 965 °C for 2 h, (c) 1.5 nm Au, annealed at 1060 °C for 0.5 h, and at 965 °C for 1 h, and (e) 1.5 nm Au annealed to 940 °C; all cooled over several hours to room temperature. The substrate is in [1–10] projection. (b) and (d) TEM images of corresponding specimens showing Au particles with $MgAl_2O_4$ necks of different heights. The halo surrounding Au particles in (b) is carbon with tungsten occupying the remaining background. They were introduced for TEM sample prep. Only carbon was used for the other specimens to reduce the risk of damage to the smaller Au nanoarticles. Inset in (b): STEM HAADF image showing the presence of an $MgAl_2O_4$ neck. (f) STEM HAADF image of Au particles without $MgAl_2O_4$ necks corresponding to specimen (e).

interfacial complexion; a reconstruction of atomic composition and arrangement in the vicinity of an interlayer that lowers the equilibrium free energy.[27] Detailed atomic models and interfacial structures, including *ab-initio* modeling of the energetics regarding this extraordinary interfacial layer and the TEM experimental details, are provided elsewhere.[26]

Systematic STEM measurements suggest that the formation of the epitaxial interfacial boundary layer strongly depends on the annealing profile. Figure 3 shows that the interface changes with increasing temperature and annealing time. Once the epitaxial complexion has formed (Figure 3(c)), further increase in annealing temperature and time does not have any apparent influence on this complexion (Figure 3(a)). This shows that this complexion is in fact an equilibrium phenomenon. The elongation at the interface in Figure 3(a) is caused by scanning instabilities; otherwise, it behaves similarly to Figure 3(c) and is consistent with our previous results.[26] Interfaces such as those shown in Figure 3(f) provide no evidence for this unique complexion. In contrast to specimens of Figures 3(b) and 3(d), they also show no sign of substrate reconfigurations in the form of pedestals beneath the Au particles.

In order to isolate the effect of gold in the growth of $MgAl_2O_4$ nanostructures, a bare magnesium aluminate substrate was annealed following a profile that would have led to the formation of Au-$MgAl_2O_4$ nanostructures in the presence of a gold overlayer. The substrate was then imaged using both SEM and AFM (Caliber, Veeco Instruments, Inc.) in tapping mode and was compared to a bare substrate that had not been annealed. The results showed that in the absence of gold, regrowth of the substrate in the form of distinct nanostructures is not present. Instead, AFM images obtained from the substrate show that through the process of annealing the surface reconfigures and forms nearly flat triangular-like terraces with an average height of 6 Å. Similar surface mass transport phenomena, which takes place well below the substrate's melting temperature of 2135 °C, have been reported for (001) $MgAl_2O_4$,[28] and for other oxide substrates such as single crystal sapphire, α-Al_2O_3.[29]

There have been reports of oxide surface reconfiguration at the local triple-junction initiated by a metal overlayer and heat.[30–33] Chatain and Carter describe this phenomenon as a means to reduce stress at the interface. Initially, the vertical component of metal-air's interfacial tension is balanced by inducing elastic stress into the substrate at the interface. Upon annealing, the resulting surface reconfigures to form ridges around dewetted metal nanoparticles, creating curvature at the metal/substrate interface.[33] In the case of gold on spinel, again initially the interfacial tension is balanced by elastic stress in the spinel (Figure 2(c)). However, upon reconfiguration, tall structures are formed beneath the gold particles (Figure 2(d)), which is a distinguishing feature of the detected mass transport.

The Au-$MgAl_2O_4$ interface at the regrown $MgAl_2O_4$ substrate constitutes of steps with heights that vary from 4 Å (1/2 the $MgAl_2O_4$ unit cell thick) along [111] spinel direction, to 5 nm as shown in Figures 4(a) and Figure 4(b). The large steps in Figure 4(a) may contain a few small steps along [1–10] direction, which we cannot identify from the

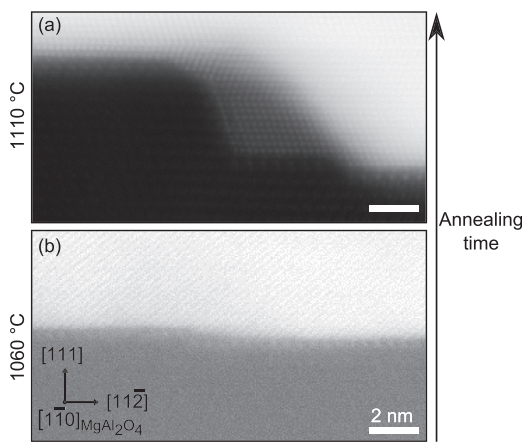

FIG. 4. HAADF STEM images illustrating Au-$MgAl_2O_4$ interfacial steps which are evident only in conjunction with Au particles that have regrown $MgAl_2O_4$ beneath them. (a) 50 nm Au, annealed at 1110 °C for 1.5 h, and at 965 °C for 2 h. (b) 1.5 nm Au, annealed at 1060 °C for 0.5 h, and at 965 °C for 1 h. The illustrated projections are the same in both (a) and (b).

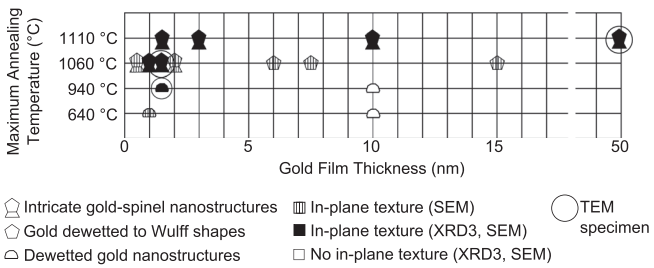

FIG. 5. Experimental results showing the existence of domains of various morphologies, and in-plane texture, indicative of conditions corresponding to $MgAl_2O_4$ growth. The in-plane texture of the gold nanoparticles was verified through XRD3 pole figures, and/or by SEM micrographs.

projected STEM-HAADF images. The formation of larger steps may be attributed to the increased annealing temperature and time as they respectively influence the diffusivity and diffusion length of atoms. We believe that these steps contribute to the mechanism behind the growth of the tall $MgAl_2O_4$ structures. A simpler annealing profile was carried out to study the details of this growth mechanism.[34]

SEM micrographs of samples where annealing has caused spinel necking structures to form show some spinel structures without an associated gold nanoparticle, as shown in Figures 1(c) or 2(b). In these cases, the necking structures are likely formed in circumstances similar to the other Au-$MgAl_2O_4$ nanostructures, with the distinction of the gold nanoparticles either evaporating or becoming unstable and diffusing away due to Oswald-like ripening.

Investigation of the combined role of temperature and thickness of the gold film on the formation of Au and Au-$MgAl_2O_4$ nanostructures is summarized in Figure 5. SEM results suggest a minimum temperature of 1060 °C is required for the epitaxial regrowth of the substrate beneath the gold nanoparticles to become evident. This minimum temperature shows an apparent increase for thicker films of gold, although this may be associated with slower dewetting and growth dynamics.[35,36] In a similar manner, delayed texture development is also evident for thicker films of gold, which can be seen in Figures 1(b) and 1(d); it is more energy intensive for atoms of larger particles (Figure 1(b)) to collectively reorganize in favor of reducing their total energy compared to their smaller counterparts (Figure 1(d)). This is clear both through comparison of their pole figures and through their morphologies; for the same temperature, the thinner film exhibits both epitaxial alignment with the underlying substrate as well as morphologies that more closely resemble equilibrium Wulff structures. Combining these observations with our STEM results shows that, by applying sufficient heat, the gold overlayer first reduces its contact area with the $MgAl_2O_4$ substrate by dewetting, and then reduces its surface energy by crystallographically aligning with the substrate. The Au induced stress at the triple junction with the substrate may be relieved through solid-state diffusion of the substrate into lower energy reconfigurations. A complexion layer at the substrate-Au interface further reduces the energy of the system.

In conclusion, through the simple process of annealing, a thin layer of gold deposited on a magnesium aluminate substrate can dewet and form crystalline gold nanostructures with majority of the particles exhibiting epitaxial alignment with the substrate. Sufficient heating conditions destabilize the Au/$MgAl_2O_4$ interface and facilitate the growth of a unique complexion. Correspondingly, the $MgAl_2O_4$ substrate regrows and forms crystalline magnesium aluminate nanostructures which contribute to the evident necking structures formed beneath the gold nanoparticles. Solid-state diffusion at the $MgAl_2O_4$ substrate surface is the most promising mechanism by which the substrate may reconfigure.

The authors acknowledge the following: The Canadian Center for Electron Microscopy (CCEM), Dr. Glynis de Silveira, Mr. Chris Butcher, Mr. Andy Duft, Mr. Travis Casagrande, Mr. Wenhe Gong, Dr. Carmen Andrei, Dr. Andreas Korinek, and Ms. Julia Huang, for their assistance, the McMaster Analytical X-Ray (MAX) Diffraction Facility, and the Brockhouse Institute for Materials Research (BIMR), Mr. Jim Garret for his assistance, and Dr. Peter Mascher for his support. The CCEM is a national facility supported by NSERC, The Canada Foundation for Innovation and McMaster University.

This work was funded by the Natural Sciences and Engineering Research Council of Canada (NSERC), and the Collaborative Research and Training Experience Program in Photovoltaics (CREATE PV).

[1]R. Sardar, A. M. Funston, P. Mulvaney, and R. W. Murray, Langmuir **25**, 13840 (2009).
[2]F. Farzinpour, A. Sundar, K. D. Gilroy, A. E. Eskin, R. A. Hughes, and S. Neretina, Nanotechnology **23**, 495604 (2012).
[3]F. Silly and M. R. Castell, Phys. Rev. Lett. **96**, 086104 (2006).
[4]C. V. Thompson, Annu. Rev. Mater. Res. **42**, 399 (2012).
[5]X. Huang, I. H. El-Sayed, W. Qian, and M. A. El-Sayed, J. Am. Chem. Soc. **128**, 2115 (2006).
[6]D. J. Gorin and F. D. Toste, Nature **446**, 395 (2007).
[7]J. T. Holland, C. Lau, S. Brozik, P. Atanassov, and S. Banta, J. Am. Chem. Soc. **133**, 19262 (2011).
[8]Y. Chen and X. Wang, Mater. Lett. **62**, 2215 (2008).
[9]C. Hrelescu, J. Stehr, M. Ringler, R. A. Sperling, W. J. Parak, T. A. Klar, and J. Feldmann, J. Phys. Chem. C **114**, 7401 (2010).
[10]K. A. Dick, Prog. Cryst. Growth Charact. **54**, 138 (2008).
[11]C. J. Murphy, L. B. Thompson, D. J. Chernak, J. A. Yang, S. T. Sivapalan, S. P. Boulos, J. Huang, A. M. Alkilany, and P. N. Sisco, Curr. Opin. Colloid Interface Sci. **16**, 128 (2011).
[12]L. Armelao, D. Barreca, G. Bottaro, G. Alberto, S. Gross, C. Maragno, and E. Tondello, Coord. Chem. Rev. **250**, 1294 (2006).
[13]G. Wang, Z. Meng, L. Jianwei, C. Li, and H. Shan, ACS Catal. **3**, 2992 (2013).
[14]W.-Z. Li, L. Kovarik, D. Mei, J. Liu, Y. Wang, and C. H. F. Peden, Nat. Commun. **4**, 2481 (2013).
[15]S.-C. Baek, K.-W. Jun, Y.-J. Lee, J. D. Kim, D. Y. Park, and K.-Y. Lee, Res. Chem. Intermed. **38**, 1225 (2012).
[16]Y. Y. Gorbanev, S. Kegnaes, and A. Riisager, Top. Catal. **54**, 1318 (2011).
[17]A. Villa, A. Gaiassi, I. Rossetti, C. L. Bianchi, K. Benthem, G. M. Veith, and L. Prati, J. Catal. **275**, 108 (2010).
[18]A. Villa, Materials **6**, 2777 (2013).
[19]J. Guo, H. Lou, H. Zhao, D. Chai, and X. Zheng, Appl. Catal., A **273**, 75 (2004).
[20]W.-C. Li, M. Comotti, A.-H. Lu, and F. Schuth, Chem. Commun. **2006**(16), 1772.
[21]T. V. W. Janssens, B. S. Clausen, B. Hvolbaek, H. Falsig, C. H. Christensen, T. Bigaard, and J. K. Norskov, Top. Catal. **44**, 15 (2007).
[22]T. V. W. Janssens, A. Carlsson, A. Puig-Molina, and B. S. Clausen, J. Catal. **240**, 108 (2006).
[23]Z. Zhange, L. Li, and J. C. Yang, J. Phys. Chem. C **117**, 21407 (2013).
[24]M. Haruta, CATTECH **6**, 102 (2002).
[25]G. A. Devenyi, J. Li, R. A. Hughes, A. C. Shi, P. Mascher, and J. S. Preston, Nano Lett. **9**, 4258 (2009).

[26]G. Zhu, T. Majdi, Y. Shao, M. Bugnet, J. S. Preston, and G. A. Botton, Appl. Phys. Lett. **105**, 231607 (2014).
[27]H. Meltzman, D. Mordehai, and W. D. Kaplan, Acta Mater. **60**, 4359 (2012).
[28]S. V. Yanina and C. B. Carter, Surf. Sci. **513**, L402 (2002).
[29]M. Yoshimoto, T. Maeda, T. Ohnishi, H. Koinuma, O. Ishiyama, M. Shinohara, M. Kubo, R. Miura, and A. Miyamoto, Appl. Phys. Lett. **67**, 2615 (1995).
[30]W. D. Kaplan, D. Chatain, P. Wynblatt, and W. C. Carter, J. Mater. Sci. **48**, 5681 (2013).
[31]D. Chatain, S. Curiotto, P. Wynblatt, H. Meltzman, W. D. Kaplan, and G. S. Rohrer, J. Cryst. Growth **418**, 57 (2015).
[32]E. Saiz, R. M. Canno, and A. P. Tomsia, Acta Mater. **48**, 4449 (2000).
[33]D. Chatain and C. Carter, Nat. Mater. **3**, 843 (2004).
[34]F. Liu, D. Xie, T. Majdi, and G. Zhu, "Twin-assisted Growth of Nominally Stable Substrates Underneath Dewetted Au Nanoparticles," Mater. Charact. (submitted).
[35]J. Mizsei and V. Lanito, J. Nanopart. Res. **3**, 271 (2001).
[36]P. R. Gadkari, A. P. Warren, R. M. Todi, R. V. Petrova, and K. Coffey, J. Vac. Sci. Technol. A **23**, 1152 (2005).